



Photoneutron emission cross sections for ^{13}C H. Utsunomiya ^{1,2}, S. Goriely,³ M. Kimura,⁴ N. Shimizu ⁵, Y. Utsuno,^{6,7} G. M. Tveten,^{8,9}
T. Renstrøm,^{8,9} T. Ari-izumi,^{1,10} and S. Miyamoto^{11,12}¹*Department of Physics, Konan University, 8-9-1 Okamoto, Higashinada, Kobe 658-8501, Japan*²*Shanghai Advanced Research Institute, Chinese Academy of Sciences, Shanghai 201210, China*³*Institut d'Astronomie et d'Astrophysique, Université Libre de Bruxelles, Campus de la Plaine, CP-226, 1050 Brussels, Belgium*⁴*Nishina Center, RIKEN, Saitama 351-0198, Japan*⁵*Center for Computational Sciences, University of Tsukuba, Tennodai Tsukuba 305-8577, Japan*⁶*Advanced Science Research Center, Japan Atomic Energy Agency, Tokai, Ibaraki 319-1195, Japan*⁷*Center for Nuclear Study, University of Tokyo, Hongo, Bunkyo-ku, Tokyo 113-0033, Japan*⁸*Department of Physics, University of Oslo, N-0316 Oslo, Norway*⁹*Expert Analytics AS, N-0179 OSLO, Norway*¹⁰*Kansai Photon Science Institute, Kizugawa, Kyoto 619-0215, Japan*¹¹*Laboratory of Advanced Science and Technology for Industry, University of Hyogo, Ako-gun, Hyogo 678-1205, Japan*¹²*Institute of Laser Engineering, Osaka University, Osaka 565-0871, Japan*

(Received 1 November 2022; accepted 8 December 2023; published 17 January 2024)

Photoneutron emission cross sections were measured for ^{13}C below $2n$ threshold using quasimonochromatic γ -ray beams produced in laser Compton scattering at the NewSUBARU synchrotron radiation facility. The data show fine structures in the low-energy tail of the giant-dipole resonance; the integrated strength of the fine structure below 18 MeV is intermediate among the past measurements with bremsstrahlung and the positron annihilation γ rays. We compare the photoneutron emission data with the TALYS statistical model calculation implemented with the simple modified Lorentzian model of $E1$ and $M1$ strengths. We also compare the total photoabsorption cross sections for ^{13}C with shell model and antisymmetrized molecular dynamics calculations as well as the statistical model calculation. We further investigate the consistency between the present photoneutron emission and the reverse $^{12}\text{C}(n, \gamma)$ cross sections through their corresponding astrophysical rate.

DOI: [10.1103/PhysRevC.109.014617](https://doi.org/10.1103/PhysRevC.109.014617)**I. INTRODUCTION**

There is growing research interest in photodisintegration cross sections in the context of the origin of ultrahigh energy cosmic rays (UHECRs). The results of the Pierre Auger [1,2] and Telescope Array [3] experiments performed in the southern and northern hemispheres, respectively, are consistent with the presence of the Greisen-Zatsepin-Kuzmi (GZK) cutoff [4,5] around 10^{20} eV, which is inferred from the pion production by protons and photodisintegration of nuclei in the interaction with the cosmic microwave background in extragalactic space. However, the analyses of the distribution of atmospheric depths at which air showers develop to their maxima showed that the composition of UHECRs is highly uncertain, largely due to different hadronic interaction models as well as scarce UHECR events [3,6]. The effect of the extragalactic propagation of UHECRs on their composition arriving at Earth is subject to photodisintegration cross sections through the giant-dipole resonance (GDR) and models of the extragalactic background light [7].

A project called PANDORA has been launched [8] to investigate photonuclear data relevant to the origin of UHECRs experimentally and theoretically. The photoreaction data required are not only photoabsorption cross sections but also partial cross sections for all decay channels of GDR by photoemissions of neutrons and charged particles for nuclei less

massive than the iron group (Fe-Co-Ni) nuclei. TALYS cross sections [9] implemented with experimental GDR parameters or theoretical dipole photon strength functions [10] are widely used [7]. However, GDR parameters are not well elucidated experimentally for the less-massive nuclei, and theoretical models often fail to predict the correct photon strength function properties.

Photonuclear data for ^{13}C compiled in the experimental nuclear data library EXFOR [11] are photoneutron [12–15] and photoproton [12,16,17] emission cross sections. The total photoabsorption cross section is also estimated from these photoneutron and photoproton cross sections [18]. In this paper, we report photoneutron emission cross sections for ^{13}C measured with quasimonochromatic γ -ray beams produced in laser Compton scattering. We discuss photonuclear data for ^{13}C in comparison with statistical model, shell model, and antisymmetrized molecular dynamics (AMD) calculations. We also discuss the stellar photodissociation rate of ^{13}C which is linked to the Maxwellian-averaged $^{12}\text{C}(n, \gamma)$ cross section by the detailed balance theorem.

II. EXPERIMENTAL PROCEDURE

Quasimonochromatic γ -ray beams were produced in the laser Compton scattering (LCS) of 1064 nm photons from

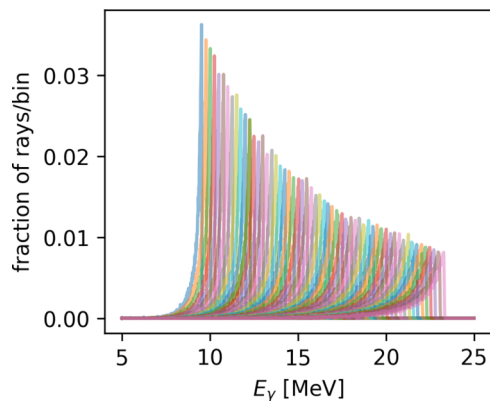


FIG. 1. The incident γ -ray beams. The profiles have been normalized and the energy bins are 10 keV.

the Inazuma Nd:YVO₄ laser with relativistic electrons in the NewSUBARU storage ring. A linear accelerator was used to inject electrons at a fixed energy of 974 MeV into the storage ring. The injected electrons were either decelerated to 743 MeV or accelerated to 1149 MeV to produce LCS γ -ray beams in the energy range of 10.01–23.48 MeV below $2n$ threshold at 23.67 MeV. The electron beam energy has been calibrated with an accuracy on the order of 10^{-5} [19,20]. The reproducibility of the electron energy is assured by automated control of the electron beam-optics parameters [19]. LCS γ -ray beams passed through two 10-cm-long Pb collimators with 3 and 2 mm apertures and were delivered to the experimental hutch GACKO (gamma collaboration hutch of Konan University).

Response functions of the LCS γ -ray beams were measured with a 3.5 in. \times 4.0 in. LaBr₃(Ce) (LaBr₃) detector. The energy profiles of the LCS γ -ray beams were determined by best reproducing the response functions in Monte Carlo simulations with GEANT4 code [21–23] that incorporates the kinematics of the LCS process, including the electron beam emittance [24,25]. The incident LCS γ -ray beams are shown in Fig. 1. Measurements were carried out in small energy increments (0.2–0.3 MeV) of the LCS γ -ray beam with the energy spread of 0.15–0.64 MeV in full width at half maximum (FWHM) or 1.5–2.8% in energy resolution. γ -ray flux was monitored with an 8 in. \times 12 in. NaI(Tl) (NaI) detector. The number of LCS γ rays was determined with the pileup or Poisson-fitting method for pulsed γ -ray beams [26,27].

The ¹³C target was in amorphous form with isotopic enrichment of 99% and chemical purity of 97%. The target material was packed into two aluminum cylindrical containers of 8 mm inner diameter with the entrance and exit windows of 25.4 μ m Kapton foils. The total areal density was 2940 mg/cm².

Photoneutrons were measured with the high-efficiency 4 π detector consisting of 10-bar ³He proportional counters of 25 mm diameter and 45 cm length that were embedded in a 36 \times 36 \times 50 cm³ polyethylene neutron moderator in three concentric rings of four, eight, and eight ³He counters at distances of 3.8, 7.0, 10.0 cm, respectively, from the axis of the LCS γ -ray beam [28]. The efficiency of the neutron

detector varies with the neutron kinetic energy. The efficiency was calibrated with a ²⁵²Cf source with the emission rate of 2.27×10^4 s⁻¹ with 2.2% uncertainty [29] and the energy dependence was determined by MCNP Monte Carlo simulations [30]. The ring ratio technique, originally developed by Berman *et al.* [31], was used to determine the average energy of neutrons emitted in the (γ , n) reaction. The average energy was used to determine the neutron detection efficiency. During the neutron measurement, the laser was periodically turned on for 80 ms and off for 20 ms in every 100 ms, to measure background neutrons. A blank target container was used to measure neutrons from the Kapton foils in every photoneutron measurement. The contribution from the Kapton foils turned out to be negligible.

III. UNFOLDING METHOD

The neutron yield cross section experimentally determined by the number of incident LCS γ rays (N_γ), the areal density of target nuclei (N_t), and the number of neutrons detected (N_n) represents a quantity that is expressed by folding the photoneutron emission cross section $\sigma(E_\gamma)$ with the energy distribution of the LCS γ -ray beam [32]):

$$\int_{S_n}^{E_{\max}} D^{E_{\max}}(E_\gamma) \sigma(E_\gamma) dE_\gamma = \frac{N_n}{N_t N_\gamma \xi \epsilon_n g} = \sigma_{\text{exp}}^{E_{\max}}. \quad (1)$$

Here, $D^{E_{\max}}$ is the normalized energy distribution of the γ -ray beam shown in Fig. 1, $\int_{S_n}^{E_{\max}} D^{E_{\max}} dE_\gamma = 1$. The quantity ϵ_n represents the neutron detection efficiency, and $\xi = (1 - e^{-\mu t})/(\mu t)$ gives a correction factor for self-attenuation in the target. The factor g represents the fraction of the γ flux above S_n .

For γ -ray energy distributions with the δ function, the integral equation [Eq. (1)] is obviously unfolded to a monochromatic cross section. Experimentally, cross sections are determined in the monochromatic approximation, which we plot at the maximum energy of the LCS γ -ray beam E_{\max} as the experimental cross section, $\sigma_{\text{exp}}^{E_{\max}}$.

Photoneutron emission cross sections $\sigma(E_\gamma)$ in Eq. (1) were unfolded at E_{\max} with the deconvolution method [32]. The method was routinely applied to the data of Ni [33], Tl [34], and Ba [35] isotopes. The maximum energy of the incident LCS γ -ray beams in the current experiment was changed in rather small increments and the interpolation was done with a third-order polynomial in numerical iterations of solving a set of linear equations (Eq. (3) of Ref. [32]) toward a convergence of the reduced χ^2 to unity. This ensures that no spurious fluctuations are caused by the choice of parameters for the cubic spline.

Furthermore, we have ensured that the unfolding did not introduce spurious structures that are due to a statistical coincidence by repeating the unfolding, where the experimental cross section measured per incident LCS γ -ray beam was randomly sampled from a Gaussian distribution with the standard deviation being the total experimental uncertainty for the measured $\sigma_{\text{exp}}^{E_{\max}}$ at E_{\max} . The fine structure has been resolved in the repeated unfolding procedure.

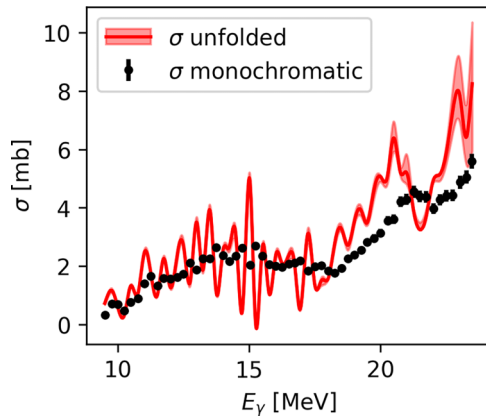


FIG. 2. Unfolded cross sections and experimental monochromatic cross sections measured per incident LCS γ -ray beam, $\sigma_{\text{exp}}^{E_{\text{max}}}$ (black dots).

Figure 2 shows unfolded cross sections in comparison with the monochromatic cross sections. Unfolded cross sections are shown by the red solid line for central values and red shaded area for uncertainties estimated by the error propagation of the 1σ uncertainty for the monochromatic cross section through the unfolding [33–35].

IV. RESULT

A. Photoneutron emission cross section

Previously photoneutron emission cross sections were measured for ^{13}C by neutron counting in irradiations with bremsstrahlung [12,13] and positron annihilation γ -ray beams [14]. Following the nomenclature of the IAEA photonuclear data library [36], these cross sections, referred to as the inclusive one-neutron emission cross section, are expressed as $\sigma(\gamma, 1nX)$, which reads $\sigma(\gamma, 1nX) = \sigma(\gamma, n) + \sigma(\gamma, np) + \sigma(\gamma, n\alpha) + \dots$, where X stands for anything except for the one detected neutron. Bremsstrahlung radiations were also used to determine (γ, p) cross sections by detecting the β activity from ^{12}B [12,16,17]. Figure 3 shows the present $(\gamma, 1nX)$ cross sections for ^{13}C in comparison with the previous data. The present data show fine structures in the low-energy tail of giant dipole resonance. The integrated strength of the fine structure below 18 MeV is lower than the positron annihilation data [14] and bremsstrahlung data of Cook *et al.* [12] and higher than the bremsstrahlung data of Koch *et al.* [13]. Above 18 MeV, the present $(\gamma, 1nX)$ cross section satisfactorily agrees with the positron annihilation data [14].

B. Photoabsorption cross section

To estimate the ^{13}C total photoabsorption cross section, different missing contributions have been added to the present photoneutron emission cross section. These include the photoproton emission as measured in [17] as well as the $(\gamma, 2n) + (\gamma, 2np)$ contribution measured in [14]. In addition, the photoneutron cross section has been supplemented at low energies with the measurement of Ref. [12] at $E < 7.5$ MeV and that of Ref. [14] at energies $E < 9.5$ MeV. All these contributions

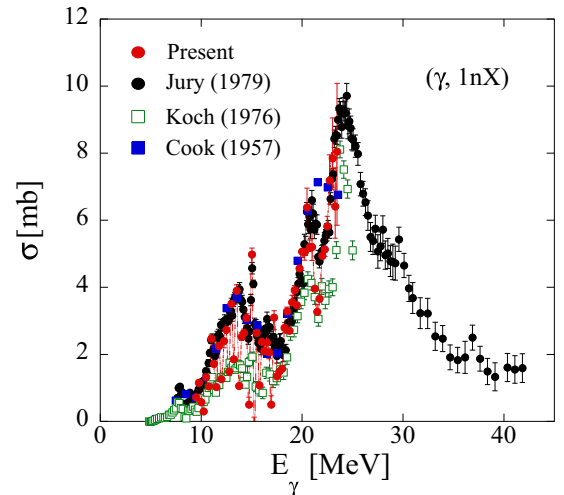


FIG. 3. Photoneutron emission cross sections, $\sigma(\gamma, 1nX)$, for ^{13}C (red filled circles). The bremsstrahlung data of [12] and [13] are shown by blue filled squares and open green squares, respectively. The data obtained with the positron annihilation γ rays [14] are shown by black filled circles.

have already been taken into account by the total photoabsorption cross section estimated in [18]. For this reason, we have used this total photoabsorption cross section for which we replaced the photoneutron cross section [14] with our newly measured cross section. The final combined cross section is shown in Fig. 4 in comparison with the one of [18].

V. DISCUSSION

A. Comparison with statistical model predictions

Based on the statistical model of Hauser and Feshbach, the TALYS code is known to be successful in estimating the cross

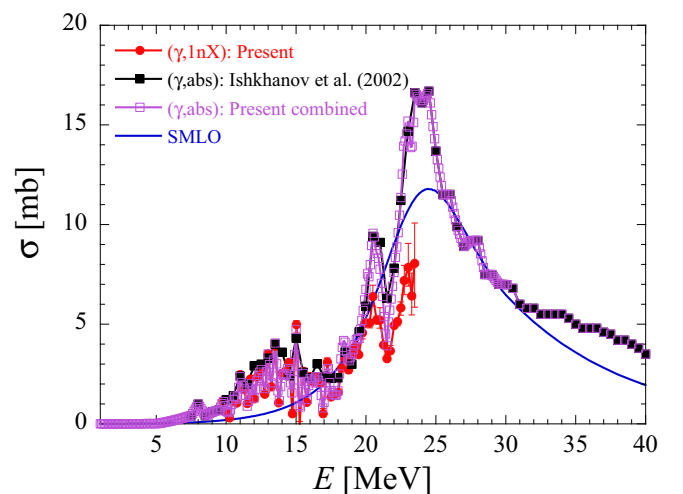


FIG. 4. Comparison of the present total photoabsorption cross section with the total photoabsorption of [18]. Photoneutron emission cross sections [12,14] used in the estimate of the photoabsorption are also shown. The blue solid line corresponds to the SMLO prediction [37].

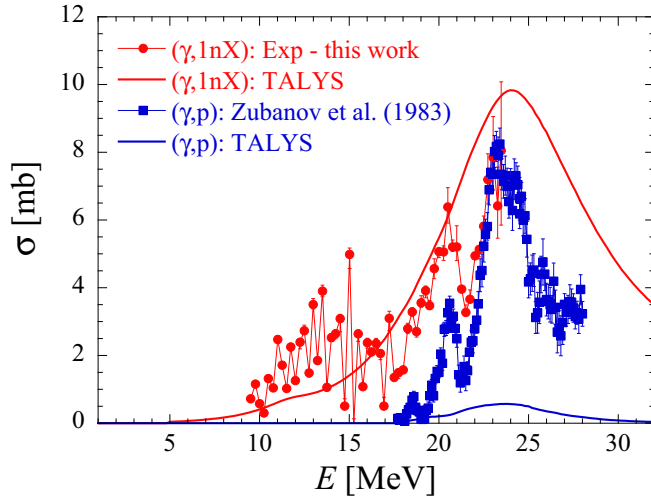


FIG. 5. Comparison of the present experimental photoneutron emission cross section (red dots) and the photoproton emission cross section of [17] with TALYS calculations based on the SMLO $E1$ and $M1$ strength functions.

section for medium-mass and heavy target nuclei. However, such a statistical approach is not well suited for the description of the reaction mechanisms taking place with light species such as ^{13}C . TALYS may still be applied and tested for this specific photoreaction. To do so, different models of the dipole strength function are available in TALYS, but for light species these models are not particularly accurate if not guided and adjusted directly on experimental data. Microscopic models of the quasiparticle random phase approximation (QRPA) type (see, e.g., Ref. [38]) are usually not extended down to elements as light as C. In contrast the simple modified Lorentzian (SMLO) model for both the $E1$ and $M1$ strength functions [37,39] can be applied. Note that, close to the $N = Z$ line, the TALYS code accounts for isospin forbidden transitions in both the single and multiple particle emission channels through a phenomenological correction reflecting the hindrance of dipole emission in self-conjugate nuclei, as introduced in Ref. [40]. While the SMLO model roughly describes the $(\gamma, \ln X)$ channel, the (γ, p) cross section is underestimated by about 1 order of magnitude. The phenomenological corrections for the isospin forbidden transitions, as explained above, affect the partial cross section predictions shown in Fig. 5, but not in a way capable of explaining the discrepancies in the (γ, p) channel between experiments and calculations. This shows how important it remains to measure the cross sections for such light species. The total photoabsorption cross section is similarly underestimated by the SMLO prediction as shown in Fig. 4.

B. Shell model calculation

Shell model calculations were carried out with the WBT interaction [41] in the $N_{\text{HO}} = 0$ to 3 valence shell, where N_{HO} stands for the harmonic-oscillator quantum number of the single-particle wave functions. This interaction is among the ones most frequently used for the p -shell region, with

two-body matrix elements fine tuned so that experimental binding energies are well reproduced. While this interaction was originally used in the pure $0\hbar\omega$, $1\hbar\omega$, and $2\hbar\omega$ model spaces within this valence shell, here we calculated the ground state and the $E1$ -excited states in the $(0 + 2)\hbar\omega$ and $(1 + 3)\hbar\omega$ spaces measured from the lowest $\hbar\omega$ state, respectively. To efficiently obtain the distribution of $E1$ excitations, we employed the Lanczos strength function method [42] with 300 Lanczos iterations. We used the standard charges, $(e_p, e_n) = ((N/A)e, -(Z/A)e)$, for calculating $E1$ strengths. The shell model calculations were performed with the KSHELL code [43]. The cross sections of photonuclear reactions were obtained with

$$\sigma(E_\gamma) = \frac{16\pi^3}{9\hbar c} \sum_v (E_v - E_{g.s.}) B(E1; g.s. \rightarrow v) f(E_\gamma; E_v, \gamma), \quad (2)$$

where $f(E_\gamma; E_v, \gamma)$ is the Lorentzian function defined by

$$f(x; x_0, \gamma) = \frac{1}{\pi} \frac{\gamma}{(x - x_0)^2 + \gamma^2}. \quad (3)$$

This function was introduced, as usual, to obtain smooth distributions from the discrete shell model spectra. We took the FWHM of $\Gamma = 2\gamma = 1$ MeV. Results of the shell model calculation for $E1$ excitations are shown in Fig. 6(a) after smoothing with $2\gamma = 1$ MeV and in Fig. 6(b) before smoothing.

C. Antisymmetrized molecular dynamics calculation

AMD calculations were carried out with the Gogny D1S density functional [44], which has been already applied to the study of the electric dipole response of neutron-rich nuclei such as ^{26}Ne [45]. The ground state is calculated with the generator coordinate method using the quadrupole deformation as the generator coordinate.

To describe the $E1$ response of ^{13}C , we employed the shifted-basis method [45], which superposes the spatially shifted single-particle wave functions. The obtained discrete energy distribution of the $E1$ strength is smeared with the Lorentzian function. The cross sections of photonuclear reactions were calculated by using the same equation with the shell model calculations, Eqs. (2) and (3) with the same parameter of $2\gamma = 1.0$ MeV. As is reported in the QRPA calculation [46], AMD calculations with the the Gogny D1S interaction also need a phenomenological correction of a shift of the $E1$ strength to lower energies due to the contribution beyond the one-particle–one-hole excitations. Results are shown in Fig. 6(a) after smoothing with $2\gamma = 1$ MeV and in Fig. 6(c) before the smoothing. An energy shift by -1.5 MeV is introduced in Figs. 6(a) and 6(c) to reproduce the peak energy of the total photoabsorption cross section.

D. Comparison with inverse (n, γ) rates

Assuming none of the ^{13}C excited states can be thermally populated, it is straightforward to estimate the total $^{13}\text{C}(\gamma, n)^{12}\text{C}$ stellar photodissociation rate from the photoneutron cross section $\sigma_{(\gamma, n)}$ on the basis of the black-body

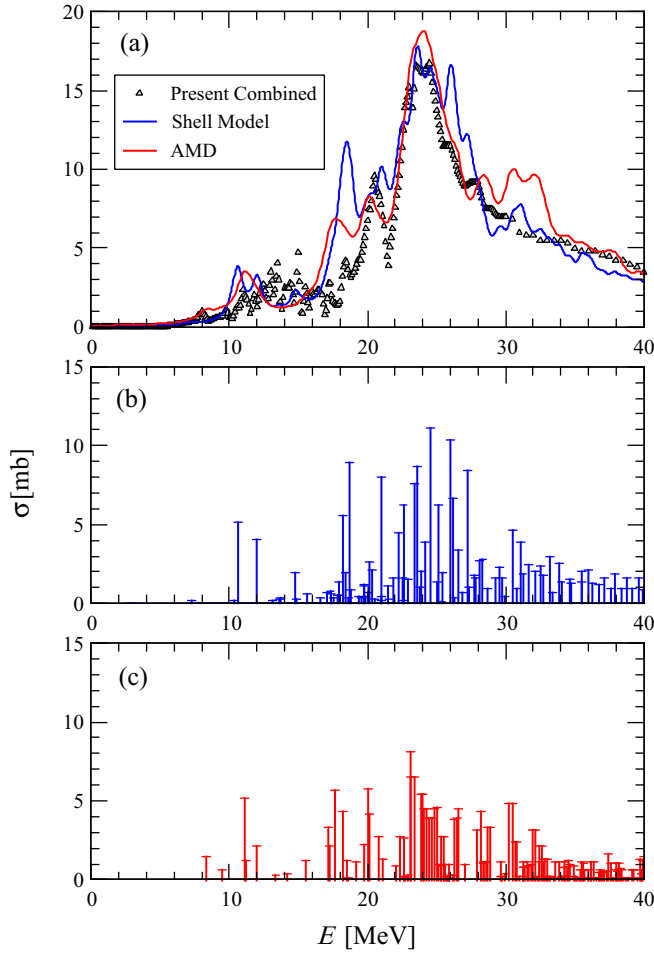


FIG. 6. (a) Results of the shell model calculation (blue) and AMD calculation (red) after smoothing with $2\gamma = 1$ MeV in comparison with the total photoabsorption cross section recommended. An energy shift by -1.5 MeV is introduced to the AMD calculation. (b) Distribution of E1 excitations in the shell model calculation with 300 Lanczos iterations. (c) Distribution of E1 excitations in the AMD calculation with an energy shift by -1.5 MeV.

Planck distribution at a given temperature $n_\gamma(E, T)$, i.e.,

$$\begin{aligned} \lambda_{(\gamma,n)}(T) &= \int_0^\infty cn_\gamma(E, T)\sigma_{(\gamma,n)}(E)dE \\ &= \frac{8\pi}{h^3c^2} \int_0^\infty \frac{E^2}{\exp(E/kT) - 1} \sigma_{(\gamma,n)}(E)dE, \end{aligned} \quad (4)$$

where c is the speed of light and h the Planck constant. To estimate the rate $\lambda_{(\gamma,n)}$, the present photoneutron cross section $\sigma_{(\gamma,n)}$ has been supplemented at low energies with the measurements of Ref. [12] at $E < 7.5$ MeV and Ref. [14] at energies $E < 9.5$ MeV.

Alternatively, making use of the detailed balance theorem, it is possible to estimate the Planck-averaged photoneutron emission rate of ^{13}C from the inverse ^{12}C radiative neutron capture rate $\langle\sigma v\rangle$, i.e.,

$$\lambda_{(\gamma,n)}(T) = \frac{G_{12\text{C}}(T)}{G_{13\text{C}}(T)} \left(\frac{mkT}{2\pi\hbar^2}\right)^{3/2} \times \langle\sigma v\rangle_{(n,\gamma)} e^{-S_n/kT}, \quad (5)$$

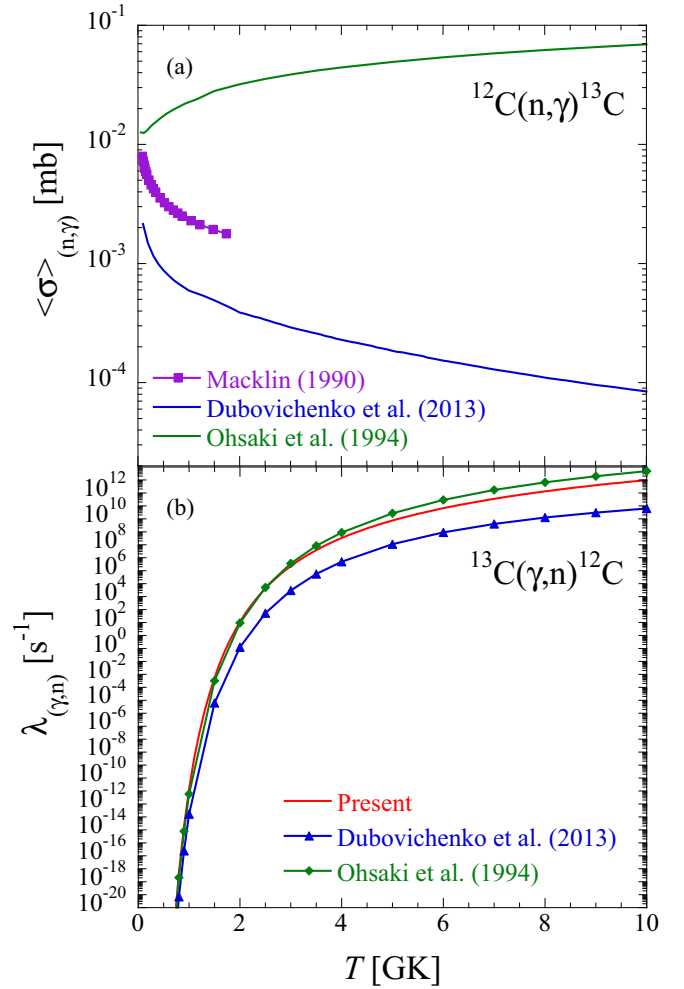


FIG. 7. (a) Experimental $^{12}\text{C}(n, \gamma)^{13}\text{C}$ Maxwellian-averaged cross sections [47–49] as a function of the temperature T . (b) Comparison between the $^{13}\text{C}(\gamma, n)^{12}\text{C}$ rates deduced from the inverse experimental cross sections of Refs. [48,49] shown in (a) and the Planck-averaged rate estimated from the present experimental photoneutron emission of ^{13}C .

where $G(T)$ is the temperature-dependent partition function, $S_n = 4.946$ MeV the neutron separation energy, m the reduced mass, and k the Boltzmann constant. The $^{12}\text{C}(n, \gamma)^{13}\text{C}$ Maxwellian-averaged cross section has been measured [47,48] and studied within the framework of the potential cluster model [49], as shown in Fig. 7. Major discrepancies exist between these different determinations, even regarding the energy dependence. These cross sections have been used to estimate the Maxwellian-averaged rate and, from it, the inverse $^{13}\text{C}(\gamma, n)^{12}\text{C}$ rate, as shown in Fig. 7(b), that can be compared with the Planck-averaged rate estimated [Eq. (4)] from the present experimental photoneutron emission of ^{13}C . The contribution of the new data above 9.5 MeV remains small compared with those in the energy range just above the neutron separation energy of 4.9 MeV. However, the new data are found still to affect the photorate shown in Fig. 5 by a factor of 2 to 6. It will be seen that the present

rate, including the SMLO extrapolation at low energies, tends to favor the $^{12}\text{C}(n, \gamma)^{13}\text{C}$ cross section measured in Ref. [48].

VI. CONCLUSION

The present measurement for ^{13}C performed below $2n$ threshold with LCS γ rays has shown the fine structure of $(\gamma, 1nX)$ cross sections in the low-energy tail of GDR. The integrated strength of the fine structure below 18 MeV is intermediate among the past bremsstrahlung [12,13] and positron annihilation [14] data. The discussion of the stellar photodissociation rate through the detailed balance theorem showed that the present photoneutron emission cross section for ^{13}C is consistent with the $^{12}\text{C}(n, \gamma)$ cross section reported in Ref. [48].

A recommended total photoabsorption cross section for ^{13}C was reconstructed based on the present data supplemented with the missing contributions from photoneutron [12,14] and photoproton [17] emission cross sections. Hauser-Feshbach statistical model calculations were performed with the TALYS code using the SMLO model of $E1$ and $M1$ strengths. While the statistical model roughly reproduced the experimental $(\gamma, 1nX)$ cross section, the model underestimated the reconstructed total photoabsorption cross section by 40% and the (γ, p) cross section by an order of magnitude. Although

TALYS cross sections are widely used in the simulation of the extragalactic propagation of UHECRs [7], the statistical nature of photodissociation cross sections needs to be further investigated for nuclei with A in a comparable mass region. The shell model and AMD calculations, with a phenomenological energy shift in the latter case, reasonably reproduce the total photoabsorption cross section for ^{13}C , showing advantage over QRPA and statistical model calculations in the predictability for light-mass nuclei relevant to the nuclear origin of UHECRs.

ACKNOWLEDGMENTS

The authors are grateful to H. Ohgaki of the Institute of Advanced Energy, Kyoto University for making a large volume $\text{LaBr}_3(\text{Ce})$ detector available for the experiment. H.U. acknowledges support from the Chinese Academy of Sciences President's International Fellowship Initiative, Grant No. 2021WM1A0025. S.G. acknowledges support from the F.R.S.-FNRS. G.M.T. acknowledges funding from the Research Council of Norway, Project Grant No. 262952. Y.U. acknowledges support from JSPS KAKENHI Grant No. 20K03981. This work was supported by the IAEA and performed in line with the IAEA CRP on "Updating the Photonuclear data Library and generating a Reference Database for Photon Strength Functions" (F41032).

-
- [1] A. Aab *et al.* (The Pierre Auger Collaboration), *Phys. Rev. Lett.* **125**, 121106 (2020).
- [2] A. Aab *et al.* (The Pierre Auger Collaboration), *Phys. Rev. D* **102**, 062005 (2020).
- [3] R. U. Abbasi, M. Abe, T. Abu-Zayyad *et al.*, *Astrophys. J.* **867**, L27 (2018).
- [4] K. Greisen, *Phys. Rev. Lett.* **16**, 748 (1966).
- [5] G. T. Zatsepin and V. A. Kuzmin, *J. Exp. Theo. Phys. Lett.* **4**, 78 (1966).
- [6] A. Aab *et al.* (The Pierre Auger Collaboration), *Phys. Rev. D* **90**, 122005 (2014).
- [7] R. A. Batista, D. Boncioli, A. di Matteo, A. van Vliet, D. Walz, *J. Cosmol. Astropart. Phys.* **10** (2015) 063.
- [8] A. Tamii *et al.*, *Eur. Phys. J. A* **59**, 208 (2023).
- [9] A. J. Koning and D. Rochman, *Nucl. Data Sheets* **113**, 2841 (2012).
- [10] R. Capote *et al.*, *Nucl. Data Sheets* **110**, 3107 (2009).
- [11] <https://www-nds.iaea.org/exfor/>.
- [12] B. C. Cook, A. S. Pemfold, and V. L. Telegdi, *Phys. Rev.* **106**, 300 (1957).
- [13] R. Koch and H. H. Thies, *Nucl. Phys. A* **272**, 296 (1976).
- [14] J. W. Jury, B. L. Berman, D. D. Faul, P. Meyer, K. G. McNeill, and J. G. Woodworth, *Phys. Rev. C* **19**, 1684 (1979).
- [15] J. G. Woodworth, K. G. McNeill, J. W. Jury, P. D. Georgopoulos, and R. G. Johnson, *Nucl. Phys. A* **327**, 53 (1979).
- [16] V. P. Denisov, A. V. Kulikov, and L. A. Kulchitskii, *J. Exp. Theo. Phys.* **19**, 1007 (1964).
- [17] D. Zubanov, R. A. Sutton, M. N. Thompson, and J. W. Jury, *Phys. Rev. C* **27**, 1957 (1983).
- [18] B. Ishkhanov, I. M. Kapitonov, E. Lileeva, E. V. Shirokov, V. Erkhkhova, M. A. Elkin, and A. Izotova, Technical Report No. MSU-INP-2002-27/711, 2002 (unpublished).
- [19] H. Utsunomiya, T. Shima, K. Takahisa, D. M. Filipescu, O. Tesileanu, I. Gheorghe, H.-T. Nyhus, T. Renström, Y.-W. Lui, Y. Kitagawa, S. Amano, and S. Miyamoto, *IEEE Trans. Nucl. Sci.* **61**, 1252 (2014).
- [20] T. Shima and H. Utsunomiya, in *Proceedings of the Nuclear Physics and Gamma-ray Sources for Nuclear Security and Non-proliferation*, Tokai, Japan, edited by T. Hayakawa *et al.* (World Scientific, Singapore, 2014), pp. 151–160.
- [21] D. Filipescu *et al.*, *Nucl. Instrum. Methods Phys. Res. Sect. A* **1047**, 167885 (2023).
- [22] D. Filipescu *et al.*, *J. Instrum.* **17**, P11006 (2022).
- [23] J. Allison *et al.*, *IEEE Trans. Nucl. Sci.* **53**, 270 (2006).
- [24] H. Utsunomiya, S. Katayama, I. Gheorghe, S. Imai, H. Yamaguchi, D. Kahl, S. Sakaguchi, T. Shima, K. Takahisa, and S. Miyamoto, *Phys. Rev. C* **92**, 064323 (2015).
- [25] D. M. Filipescu, I. Gheorghe, H. Utsunomiya, S. Goriely, T. Renström, H.-T. Nyhus, O. Tesileanu, T. Glodariu, T. Shima, K. Takahisa, S. Miyamoto, Y.-W. Lui, S. Hilaire, S. Péru, M. Martini, and A. J. Koning, *Phys. Rev. C* **90**, 064616 (2014).
- [26] H. Utsunomiya, T. Watanabe, T. Ari-izumi, D. Takenaka, T. Araki, K. Tsuji, I. Gheorghe, D. M. Filipescu, S. Belyshev, K. Stopani, D. Symochko, H. Wang, G. Fan, T. Renström, G. M. Tveten, Y.-W. Lui, K. Sugita, and S. Miyamoto, *Nucl. Instrum. Methods Phys. Res. Sect. A* **896**, 103 (2018).
- [27] T. Kondo, H. Utsunomiya, H. Akimune, T. Yama-gata, A. Okamoto, H. Harada, F. Kitatani, T. Shima, K. Horikawa, and S. Miyamoto, *Nucl. Instrum. Methods Phys. Res. Sect. A* **659**, 462 (2011).
- [28] O. Itoh, H. Utsunomiya, H. Akimune, T. Kondo, M. Kamata, T. Yamagata, H. Toyokawa, H. Harada, F. Kitatani, S. Goko, C. Nair, and Y.-W. Lui, *J. Nucl. Sci. Technol.* **48**, 834 (2011).

- [29] H.-T. Nyhus, T. Renstrøm, H. Utsunomiya, S. Goriely, D. M. Filipescu, I. Gheorghe, O. Tesileanu, T. Glodariu, T. Shima, K. Takahisa, S. Miyamoto, Y.-W. Lui, S. Hilaire, S. Péru, M. Martini, L. Siess, and A. J. Koning, *Phys. Rev. C* **91**, 015808 (2015).
- [30] J. F. Briesmeister, *MCNP, A General Monte Carlo N-Particle Transport Code*, Version 4B (Los Alamos National Laboratory, Los Alamos, NM, 1997).
- [31] B. L. Berman, J. T. Caldwell, R. R. Harvey, M. A. Kelly, R. L. Bramblett, and S. C. Fultz, *Phys. Rev.* **162**, 1098 (1967).
- [32] T. Renstrøm, H. Utsunomiya, H. T. Nyhus, A. C. Larsen, M. Guttormsen, G. M. Tveten, D. M. Filipescu, I. Gheorghe, S. Goriely, S. Hilaire, Y.-W. Lui, J. E. Midtbø, S. Péru, T. Shima, S. Siem, and O. Tesileanu, *Phys. Rev. C* **98**, 054310 (2018).
- [33] H. Utsunomiya, T. Renstrøm, G. M. Tveten, S. Goriely, S. Katayama, T. Ari-izumi, D. Takenaka, D. Symochko, B. V. Kheswa, V. W. Ingeberg, T. Glodariu, Y.-W. Lui, S. Miyamoto, A. C. Larsen, J. E. Midtbø, A. Gørgen, S. Siem, L. Crespo Campo, M. Guttormsen, S. Hilaire, S. Péru, and A. J. Koning, *Phys. Rev. C* **98**, 054619 (2018).
- [34] H. Utsunomiya, T. Renstrøm, G. M. Tveten, S. Goriely, T. Ari-izumi, D. Filipescu, J. Kaur, Y.-W. Lui, W. Luo, S. Miyamoto, A. C. Larsen, S. Hilaire, S. Péru, and A. J. Koning, *Phys. Rev. C* **99**, 024609 (2019).
- [35] H. Utsunomiya, T. Renstrøm, G. M. Tveten, S. Goriely, T. Ari-izumi, V. W. Ingeberg, B. V. Kheswa, Y.-W. Lui, S. Miyamoto, S. Hilaire, S. Péru, and A. J. Koning, *Phys. Rev. C* **100**, 034605 (2019).
- [36] T. Kawano *et al.*, *Nucl. Data Sheets* **163**, 109 (2020).
- [37] V. Plujko, O. Gorbachenko, R. Capote, and P. Dimitriou, *At. Data Nucl. Data Tables* **123-124**, 1 (2018).
- [38] S. Goriely and V. Plujko, *Phys. Rev. C* **99**, 014303 (2019).
- [39] S. Goriely, S. Hilaire, S. Péru, and K. Sieja, *Phys. Rev. C* **98**, 014327 (2018).
- [40] J. A. Holmes, S. E. Woosley, W. A. Fowler, and B. A. Zimmerman, *At. Data Nucl. Data Tables* **18**, 305 (1976).
- [41] E. K. Warburton and B. A. Brown, *Phys. Rev. C* **46**, 923 (1992).
- [42] E. Caurier, G. Martínez-Pinedo, F. Nowacki, A. Poves, and A. P. Zuker, *Rev. Mod. Phys.* **77**, 427 (2005).
- [43] N. Shimizu, T. Mizusaki, Y. Utsuno, and Y. Tsunoda, *Comput. Phys. Commun.* **244**, 372 (2019).
- [44] J. F. Berger, M. Girod, and D. Gogny, *Comput. Phys. Commun.* **63**, 365 (1991).
- [45] M. Kimura, *Phys. Rev. C* **95**, 034331 (2017).
- [46] S. Peru and M. Martini, *Eur. Phys. J. A* **50**, 88 (2014).
- [47] R. Macklin, *Astrophys. J* **357**, 649 (1990).
- [48] T. Ohsaki, Y. Nagai, M. Igashira, T. Shima, K. Takeda, S. Seino, and T. Irie, *Astrophys. J.* **422**, 912 (1994).
- [49] S. Dubovichenko, A. Dzhaairov-Kakhramanov, and N. Burkova, *Int. J. Mod. Phys. E* **22**, 1350028 (2013).